ISSN 1027-4510, Journal of Surface Investigation: X-ray, Synchrotron and Neutron Techniques, 2023, Vol. 17, No. 6, pp. 1356–1363. © Pleiades Publishing, Ltd., 2023.
Russian Text © The Author(s), 2023, published in Poverkhnost', 2023, No. 12, pp. 46–53.

Silicon Microstrip Detector for Studying Fast Processes on a Synchrotron Beam

V. M. Aulchenko[a], A. A. Glushak[a, c, d], V. V. Zhulanov[a], A. N. Zhuravlev[a, c], V. A. Kiselev[a], V. N. Kudryavtsev[a, b], P. A. Piminov[a, c], V. M. Titov[a], and L. I. Shekhtman[a, b, d, *]

[a] *Budker Institute of Nuclear Physics, Siberian Branch, Russian Academy of Sciences, Novosibirsk, 630090 Russia*
[b] *Novosibirsk State University, Novosibirsk, 630090 Russia*
[c] *Center for Collective Use "Siberian Circular Photon Source" (SKIF), Boreskov Institute of Catalysis, Russian Academy of Sciences, Novosibirsk, 630090 Russia*
[d] *Tomsk State University, Tomsk, 634050 Russia*
**e-mail: L.I.Shekhtman@inp.nsk.su*

Received January 12, 2023; revised March 20, 2023; accepted March 20, 2023

Abstract—In this paper, we describe the current state of development of a prototype detector for the study of fast processes (DIMEX) based on a silicon microstrip sensor. The silicon microstrip sensor is made of *n*-type silicon with *p*-type implants in the form of strips. Aluminum contacts with microwelding pads at the ends are applied to the strips along the entire length. The signals from the strips are read using a DMXS6A integrated circuit specially designed for this project, which contains six recording electronic channels with a dark-current compensation circuit at the input, four integrators, 32 analog memory cells, and an analog shift register. Each sensor strip is connected to the guard ring through a 400-Ω resistor and to the recording-channel input through a 100-kΩ resistor. This resistive divider at the input of the recording channel makes it possible to adapt the dynamic range of the recording microcircuit integrator to the full range of photon-flux changes in synchrotron-radiation output channel no. 8 of the VEPP-4M storage ring equipped with a nine-pole wiggler with a field of 1.95 T as the source of synchrotron radiation. Measurements of the dynamic range of the DIMEX-Si prototype show that the maximal flux that can be recorded in the linear mode exceeds 10^5 photons/channel from each electron bunch in the storage ring. The ability of the detector to detect signals from bunches following after 55 ns in the multi-bunch mode, which simulates the operation of the 4+-generation synchrotron-radiation source Siberian Circular Photon Source (SKIF) under construction in the Novosibirsk region, on which such a detector is planned to be used, is also demonstrated.

Keywords: fast processes, detonation processes, coordinate detectors, time-resolved detectors, electronic recording channel, microstrip silicon detector, specialized integrated circuit, synchrotron radiation

DOI: 10.1134/S1027451023060253

INTRODUCTION

At the Center for Collective Use "Siberian Center for Synchrotron and Terahertz Radiation" (CCU SCSTR), the Budker Institute of Nuclear Physics, Siberian Branch, Russian Academy of Sciences, developing methods for studying fast processes using synchrotron radiation (SR) beams are being actively studied. The stations "Submicrosecond Diagnostics" and "Extreme State of Matter" [1–3] operate on two SR sources used at CCU SCSTR, the VEPP-3 and VEPP-4M storage rings.

The main recording device at both the stations is the DIMEX-G (Detector for imaging of explosions) detector based on a multi-element high-pressure gas-ionization chamber filled with a mixture of Xe + 25% CO_2 at 7 atm [4–9]. DIMEX-G records SR signals from each bunch of electrons in the storage ring and writes them to the internal memory until the signal from the next bunch appears. Thus, this detector records an image of a shadow from a fast-moving object every 125 ns at the VEPP-3 (two-bunch mode) and every 200 ns at the VEPP-4M (six-bunch mode). DIMEX-G is a single-coordinate detector with 512 channels spaced at 100 μm. The maximal signal that the detector can record in the linear mode corresponds to a flux of ~2000 photons/channel from a single electron bunch (photon energy is 20 keV). The detector can record up to 100 frames during the experiment, and the maximal recording frequency is 10 MHz. The spatial resolution of DIMEX-G is 250 μm at an average photon energy in the SR spectrum of 20 keV, and the quantum efficiency reaches 40%.

DIMEX-G has been effectively used for more than 17 years at VEPP-3 and for more than seven years at VEPP-4M to study detonation and shock-wave pro-

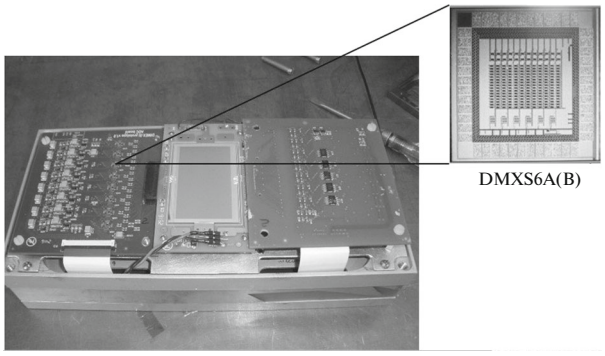

Fig. 1. Image of the DIMEX-Si prototype with the topology of the specialized DMXS6A IC for detecting radiation (inset).

cesses [10–13]. However, this detector has a number of significant limitations, and further improvement of its parameters requires significant changes in the design of both the detecting element itself and the recording electronics. For example, the maximal photon flux that DIMEX-G can detect is limited due to the accumulation of the space charge of ions in the gas. The maximal frame-recording rate is limited due to the low drift rate and longitudinal electron diffusion, as well as due to the insufficient speed of the recording electronics. The spatial resolution is limited by the transverse diffusion of electrons in the gas. All these problems can be solved by switching from gas technology to a solid-state one and by replacing the gas-ionization chamber with a silicon microstrip detector with high-speed recording electronics [14–19]. Unlike xenon, where ions are more than three orders of magnitude slower than electrons, the mobility of holes in silicon is only half that of electrons. Also, the carrier mobility itself in silicon is higher than that in gas while the electric-field strengths in the silicon sensor and in the gas gap are close. Thus, the space-charge effects in a silicon sensor will manifest themselves at a significantly higher photon flux than in a gas detector.

PROTOTYPE OF THE SILICON MICROSTRIP DETECTOR

To study the main parameters of a detector based on a silicon microstrip sensor, a DIMEX-Si prototype was created [16–18] (Fig. 1). The prototype includes a silicon sensor with a sensitive area of 30 × 51 mm that is manufactured by Hamamatsu Photonics. The sensitive area is covered with 512 strips with a length of 30 mm that are spaced 50 μm from each other. Each strip is a *p*-type implant on *n*-type silicon coated with an aluminum metal contact. The sensor thickness is 320 μm. The strips are connected to a grounded guard ring via 400-Ω resistors. The bias voltage applied to the common electrode on the opposite side of the sensor is 300 V.

In the central part of the sensor, 96 strips are connected by microwelding to the recording electronics based on a DMXS6A(B) specialized integrated circuit (IC) developed specifically for this project [19]. The IC contains six channels, each including a voltage-to-current converter, a dark-current compensation circuit, four integrators with a reset circuit, 32 analog memory cells (8 cells per integrator), and an output analog shift register (Fig. 2). There is a 10-kΩ resistor in series at the input of each channel (later increased to 100 kΩ as is shown below). A 400-Ω resistor on the sensor and a 10-kΩ (100 kΩ) resistor on the recording board provide current attenuation to the channel of DMXS6A(DMXS6B) IC to adapt the dynamic range of the integrators to the range of the detected photon flux in the sensor.

The DIMEX-Si prototype with the first version of the DMXS6A IC was studied earlier in [17–19]. It was shown that the silicon microstrip detector indeed makes it possible to increase significantly the maximal recorded photon flux from a single bunch of electrons in the storage ring and improve the spatial and temporal resolution while the new recording electronics make it possible to increase the frame rate up to 40 MHz. However, a significant drawback of the new IC was a high noise level, which did not allow an increase in the signal-to-noise ratio compared to that in a gas detector [18, 19]. As a result of modeling and further analysis, a source of increased noise was found. It turned out to be a dark-current compensation circuit. In this scheme, the amplifier output in the feedback circuit remained connected to the control input of the compensating current generator during exposure. At the same time, the input of the feedback amplifier in this phase was disconnected from the signal circuit. Consequently, the noise at the output of the feedback amplifier increased significantly, resulting in a corresponding increase in the compensation-current noise. In the new version of the DMXS6B IC, a switch was added to the dark-current compensation circuit that turns off the amplifier output in feedback from the control input of the compensation-current generator. The feedback voltage was maintained on a special capacitance connected to the control input of the compensation-current generator. A new version of the IC was produced in 2021, and all measurements described here are made with the DIMEX-Si prototype with recording electronics based on the DMXS6B IC.

TEST RESULTS OF THE DIMEX-Si PROTOTYPE WITH THE NEW DMXS6B IC

To measure the magnitude of the noise and compare the noise in the new version of the recording IC with the old version, data without irradiating the detector were collected. Comparison of the signal-distribution histograms in these measurements is shown in Fig. 3 for DMXS6A (Fig. 3a) and DMXS6B (Fig. 3b).

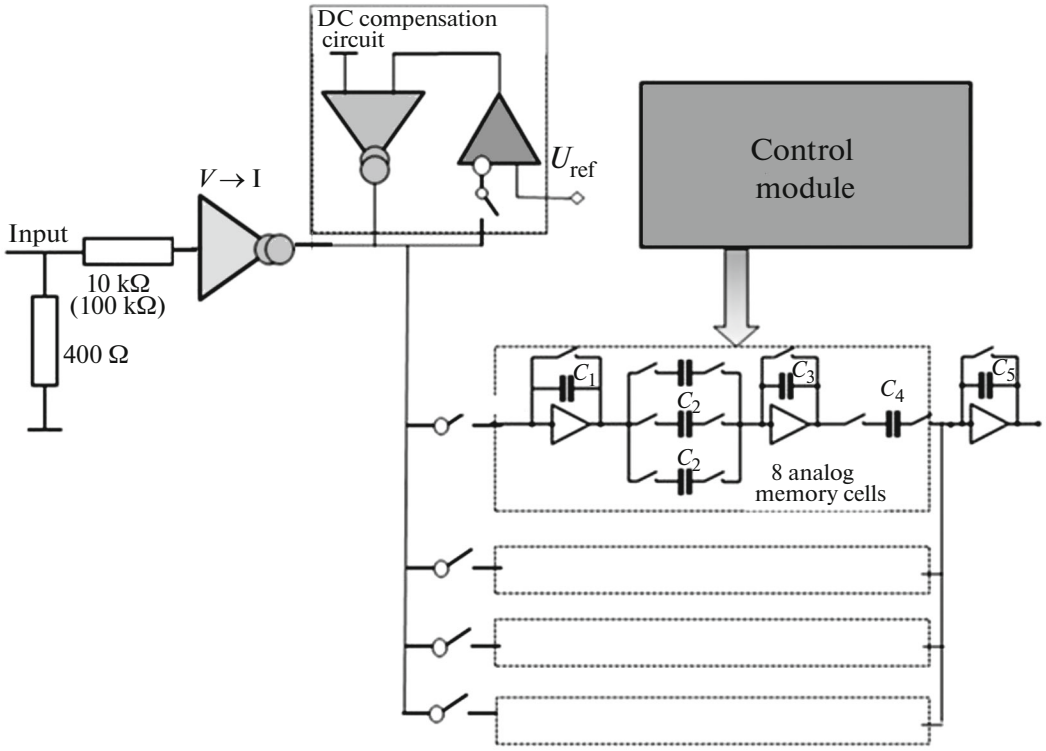

Fig. 2 Block diagram of the DMXS6A IC with a resistive divider at the input of the recording channel (not included in the IC).

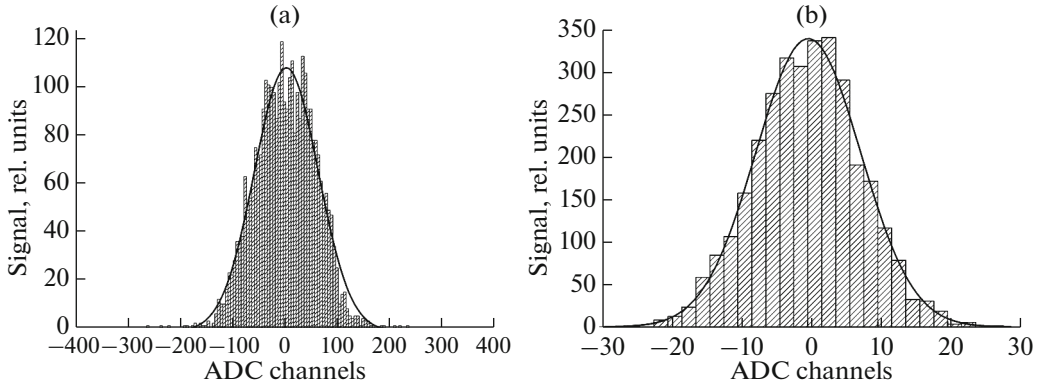

Fig. 3. Histograms of the noise signal distribution obtained without detector irradiation in two versions of the recording IC: (a) DMXS6A, the standard deviation of the noise distribution is equal to 61 ADC channels, (b) DMXS6B, the standard deviation of the noise distribution is equal to 7.5 ADC channels.

Noise (standard deviation of the signal distribution) with the new version of the IC decreased by eight times, from 61 to 7.5 bins of an analog-to-digital converter (ADC).

To measure the dependence of the signal in the detector on the absorbed photon flux, the detector was irradiated with a SR flux. The photon flux incident on the detector was set by changing the height of the collimator aperture. The total energy absorbed in a silicon sensor with a thickness of 320 μm was preliminarily measured using a monitor detector with exactly the same sensor as that in the DIMEX-Si. In the monitor detector, one strip was connected to the input of an oscilloscope and, thus, it was possible to measure the total charge flowing through one channel of the detector when photons from one electron bunch were absorbed. This measurement was carried out at one fixed height of the collimator aperture, then the photon flux was calculated based on the known height of the collimator hole and the calculated average photon energy in the absorbed radiation spectrum, which is equal to 17 keV for the detector position perpendicular

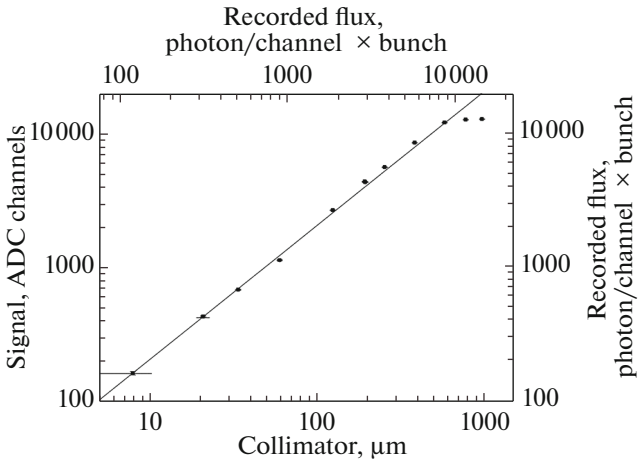

Fig. 4. Dependence of the signal in the detector with the DMXS6A IC on the height of the collimator aperture and the absorbed photon flux. The scales at the top and on the right show compliance with absorbed flux calculations based on monitor detector measurements and using electronic calibration, respectively.

to the beam. Figure 4 shows the result of measuring the dependence of the signal in the detector on the height of the collimator hole (lower scale) and the photon flux (upper scale). Besides, the photon flux was also calculated using electronic calibration (right scale). To do this, a known signal was applied to the input of the recording channel, and the calibration constant was calculated from the value of the output signal, which determines the value of the ADC bin in charge units at the input. As can be seen in Fig. 4, the flux calculated using electronic calibration agrees with the result obtained using measurement with the monitor detector with an accuracy of ~10%.

As can be seen in Fig. 4, the signal saturates at a flux of ~10000 photons per channel from one bunch. This is due to the overloading of integrators in the recording IC. In this measurement, 10-kΩ resistors were included at the input of the recording channels. Thus, in order to achieve the maximal recorded flux of 10^5 photons/channel from one bunch, it is necessary to reduce the input current tenfold more, for which the resistors at the channel inputs must be increased to 100 kΩ. It should be noted that the intrinsic noise of the recording channel equal to 7.5 bins of ADC (Fig. 3) corresponds to ~7 photons with an energy of 17 keV. Thus, the statistical signal fluctuations equal to 100 photons at the maximal recorded flux of 10000 photons significantly exceed the channel's own noise. The photon flux, at which the statistical noise is comparable to the channel's own noise, is 49 photons/channel. If this value of the photon flux is taken as the lower limit of the dynamic range, then the width of the dynamic range of the detector in this mode is ~200. In the mode with the input current attenuated by a factor of ten, the channel's own noise of 7.5 bins of ADC corresponds to statistical fluctuations in the flux of ~70 photons. In this case, the flux value, at which the statistical noise is comparable to the channel's own noise, is, respectively, 4900 photons/channel. Since the maximal limit of the dynamic range reaches 10^5 photons/channel, the width of the dynamic range in this case is ~20.

For additional verification of the correctness of the estimated flux and noise values, images of a low-contrast test object were taken (Fig. 5a). The test object is a poly(methyl methacrylate) block with four steps with a height of 1 mm and a width of 2.5 mm. The data received from the detector is a set of 32 arrays of 96 numbers. Each number is a signal received from the corresponding detector channel. An array of 96 num-

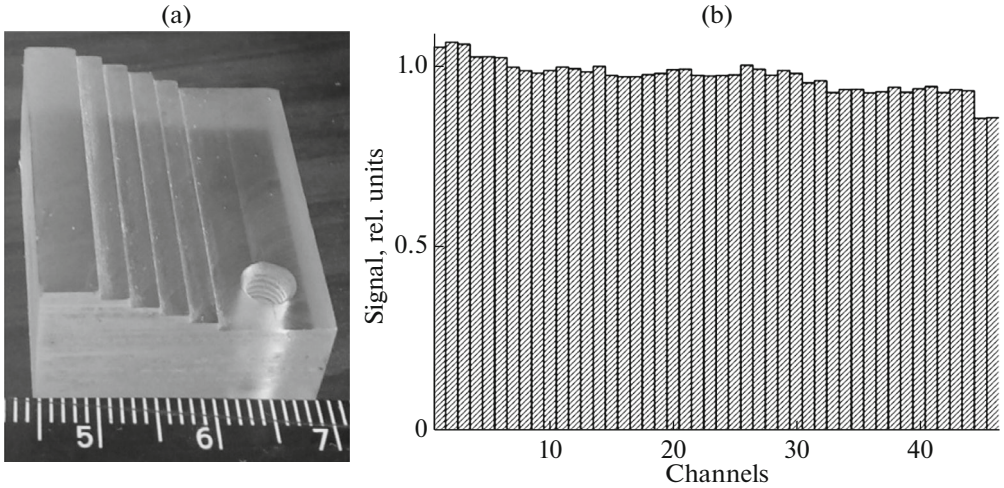

Fig. 5. (a) Appearance of the test object and (b) image of the test object obtained with the help of SR in the mode with a maximal recorded photon flux of 10000 photons/channel.

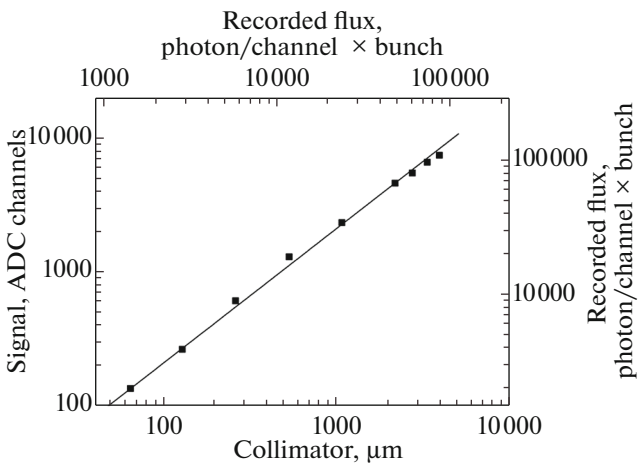

Fig. 6. Dependence of the signal in the detector with the DMXS6B IC on the height of the collimator aperture and the absorbed photon flux with increased resistors at the input of the recording channels. The scales at the top and on the right show compliance with absorbed flux calculations based on monitor detector measurements and using electronic calibration, respectively. The measurement was carried out at a perpendicular position of the detector with respect to the SR beam.

bers corresponds to the signal received from one SR flash; we will further call such an array a frame. The whole set of 32 frames will be called a film. To obtain an image of the test object, the data obtained without detector irradiation were subtracted from the primary data obtained by exposure of the test object to SR. Next, the data were normalized to the "flat field" image, i.e., on the result of exposure of the detector without a test object with increased statistics. To obtain a flat-field image, 100 films were made in a mode identical to the exposure mode of the test object, and the averaged result was used for normalization. A one-dimensional image of the test object is shown in Fig. 5b. As can be seen in the figure, the contrast of a 1-mm-high polymethyl-methacrylate step is approximately 5% while the photon-flux value calculated from the magnitude of signal fluctuations (flux equivalent to noise, NEQ) is approximately 10000 photons/channel.

To obtain the maximal recorded flux of 10^5 photons/channel, the resistors at the input of the recording channels were changed from 10 to 100 kΩ, and all subsequent measurements were carried out with a modified version of the recording electronics. The result of measuring the dependence of the signal on the recorded photon flux is shown in Fig. 6. As can be seen in the figure, a flux of 10^5 photons can be recorded in this mode at the very edge of the linear range of the integrators.

An important parameter of the detector is its temporal resolution and the limiting frame rate. These parameters are related to each other since the detector's temporal resolution determines the minimal time required to expose and record the signal from one SR flash into analog memory. The temporal resolution and the limiting frame rate are mainly determined by the parameters of the recording IC since the current pulse from the sensor strip from a single SR flash lasts only a few ns. The time resolution of the detector with the DMXS6B IC was studied by measuring the dependence of the signal in several adjacent frames on the delay between the sync pulse, which sets the beginning of the sequence of signals that control IC operation and the moment of SR flashes. The results of these measurements for detectors with the first version of the DMXS6A IC and with the new version of the DMXS6B IC are compared in Fig. 7.

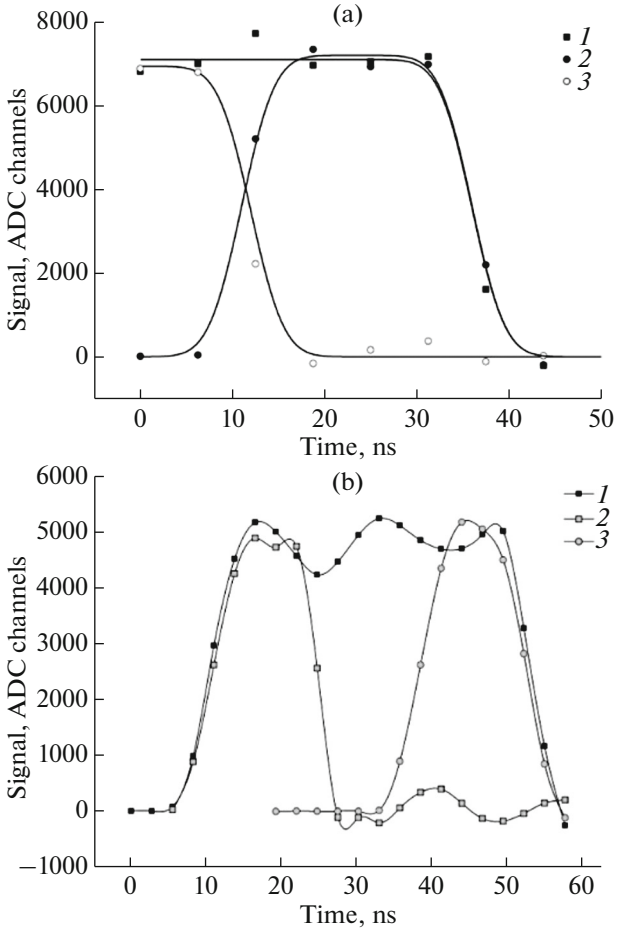

Fig. 7. Dependence of the signal in two adjacent frames on the delay between the detector sync pulse and the moment of the SR flash in the detector: (a) with the DMXS6A IC, (*1*) the frame-exposure time is 50 ns, frame no. 19; (*2*) frame-exposure time is 25 ns, frame no. 18; and (*3*) frame-exposure time is 25 ns, frame no. 19; (b) with the DMXS6B IC, (*1*) frame-exposure time 55 ns, frame no. 9; (*2*) frame-exposure time is 27.5 ns, frame no. 9; and, (*3*) frame exposure time is 27.5 ns, frame no. 8.

The time resolution of the detector is the duration of the transition phase from the zero signal to the max-

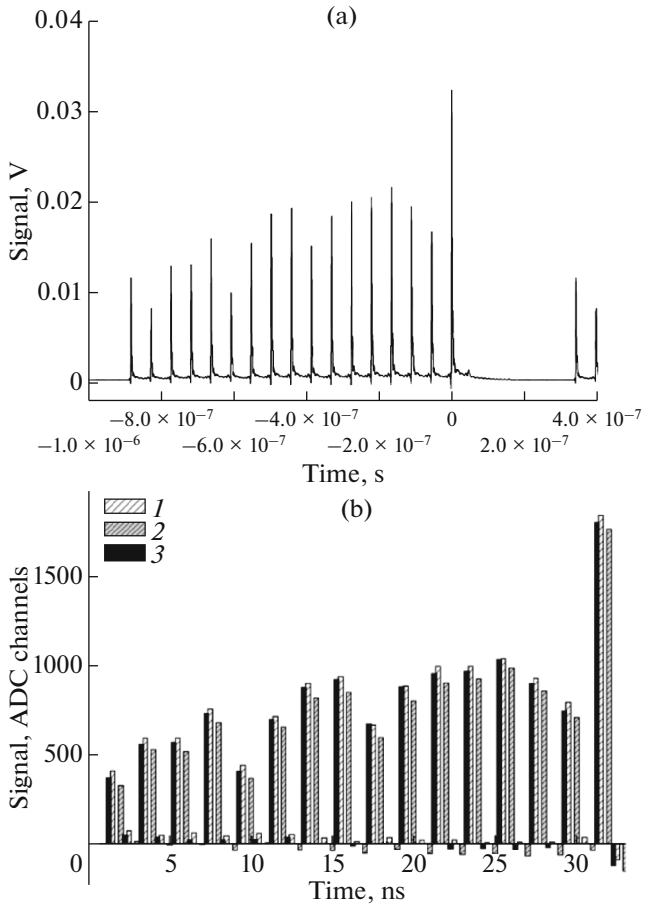

Fig. 8. Operation of DIMEX-Si in the multi-bunch mode: (a) signal oscillogram from one monitor detector strip, (b) signal in one channel in three successive DIMEX-Si films.

imal signal in the frame. This time is equal to the convolution of the duration of the current pulse from the sensor strip and the time constant of the integrator (rising edge), which is determined by the upper limit of the frequency band. In both IC versions, this time is approximately 7 ns. In the first IC version, there was a phase in the time sequence of signals when the signal is not equal to zero in both adjacent frames. In this phase, two integrators are simultaneously connected to the input signal. In the DMXS6B IC, this phase was removed. It should be noted that the first integrator is disconnected earlier while the second integrator is connected later than in those in DMXS6A. This led to the appearance of a phase, in which the signal is absent in both the first and second frames. This feature of the timing diagram helped to additionally reduce the noise level. However, because of this, the duration of the phase of the maximal signal in the frame was significantly reduced, which is only ~5 ns at a frame-repetition period of 27.5 ns. The short duration of the phase of the maximal signal in a frame means that the requirements for the stability of the detector sync pulses with respect to the flight of bunches in the storage ring must be increased. Besides, this means that the maximal recording frame rate cannot exceed 40 MHz.

For operation with DIMEX-Si, there must be a sequence of electron bunches created in the storage ring, the distance between which is equal to or a multiple of the frame repetition period in the detector. The dark-current compensation circuit, which provides a stable zero signal level in the absence of irradiation, must be disabled during exposure. It is important that at the time of turning off, there is no signal from the sensor at the inputs of the recording channels. To do this, there must be a break of 200–300 ns in the sequence of electron bunches in the storage ring. To study the possibility of operating the detector in a multi-bunch mode, a mode with a sequence of 17 electron bunches following with an interval of 55 ns was implemented in the VEPP-4M. In the first measurement in this mode, it was important to understand the fundamental possibility of operation, which, in particular, is determined by the properties of the dark-current compensation circuit. Figure 8a shows an oscillogram of the signal from one strip of the silicon monitor detector, which shows the time dependence of the sensor current.

Figure 8a shows signals from 17 bunches with various currents and a break in their sequence with a duration of about 330 ns. For stable operation of the DMXS6B IC, the dark current compensation circuit must be turned off before exposure begins during this break. Figure 8b shows the signals in one of the detector channels in three successive films. The detector operated with a frame rate equal to half the distance between the bunches in order to see how well the signals from different bunches can be separated, as well as what the signal level is in the absence of radiation between the bunches. Figure 8b shows that the signal fluctuates from frame to frame by ~10%. Both the signal level in the frames corresponding to the flight of the bunch and the signal level in the frames where there is no change in irradiation. This indicates the presence of instability of the sync pulses that control detector operation with respect to the moments of flight of the bunches, as well as a possible nonoptimal position in time of the moment of turning off the dark-current compensation circuit. These issues require further study.

CONCLUSIONS

The new version of the DMXS6B recording IC significantly reduced the noise level in the DIMEX-Si prototype detector. Tests of the SR beam detector on the VEPP-4M storage ring showed that the maximal photon flux that can be recorded in the linear mode

with a series resistor of 10 kΩ at the recording-channel input (IC DMXS6A) is 10^4 photons/channel from one electron bunch. At an increase in the resistance of the resistors to 100 kΩ and a corresponding decrease in the fraction of current flowing from the sensor to the input of the recording channels, the maximal recorded flux increases tenfold and reached 10^5 photons/channel from one electron bunch (DMXS6B IC). This result is extremely important from the point of view of increasing the accuracy of measurements using the DIMEX-Si detector in experiments.

The time resolution of the detector with the new version of the recording IC remained the same as that with the first IC version. The timing diagram of the recording-channel operation in the new IC version was changed in such a way that now more precise tuning and stabilization of the detector-storage synchronization operation is required. In the future, when developing a full-scale integrated circuit for the final version of the detector, it is necessary to take into account the emerging problem and make it possible to adjust flexibly the parameters of the IC timing diagram.

In measurements, the multi-bunch mode was implemented for the first time in the VEPP-4M storage ring. The fundamental possibility of operation of the DIMEX-Si detector in the mode with filling of the storage ring with electron bunches following after 55 ns, with a break in the bunch sequence with a duration of ~330 ns, is demonstrated. A similar mode will be implemented in the SKIF synchrotron-radiation source.

FUNDING

The work on measuring the characteristics of the DIMEX-Si detector was partially supported by the Government of the Russian Federation, agreement no. 075-15-2022-1132 in accordance with Decree 220 of April 9, 2010.

CONFLICT OF INTEREST

The authors state that they have no conflicts of interest.

REFERENCES

1. B. P. Tolochko, A. V. Kosov, O. V. Evdokov, I. L. Zhogin, K. A. Ten, E. R. Pruuel, L. I. Shekchtman, V. M. Aulchenko, V. V. Zhulanov, P. F. Piminov, V. P. Nazmov, K. V. Zolotarev, and G. N. Kulipanov, Phys. Procedia **84**, 427 (2016). https://www.doi.org/10.1016/j.phpro.2016.11.072
2. P. A. Piminov, G. N. Baranov, A. V. Bogomyagkov, D. E. Berkaev, V. M. Borin, V. L. Dorokhov, S. E. Karnaev, V. A. Kiselev, E. B. Levichev, O. I. Meshkov, S. I. Mishnev, S. A. Nikitin, I. B. Nikolaev, S. V. Sinyatkin, P. D. Vobly, K. V. Zolotarev, and A. N. Zhuravlev, Phys. Procedia **84**, 19 (2016). https://www.doi.org/10.1016/j.phpro.2016.11.005
3. V. M. Aulchenko, V. V. Zhulanov, G. N. Kulipanov, K. A. Ten, B. P. Tolochko, and L. I. Shekhtman, Phys.—Usp. **61**, 515 (2018). https://www.doi.org/10.3367/UFNe.2018.01.038339
4. V. Aulchenko, P. Papushev, S. Ponomarev, L. Shekhtman, and V. Zhulanov, J. Synchrotron Radiat. **10**, 361 (2003). https://www.doi.org/10.1107/S0909049503009142
5. V. Aulchenko, O. Evdokov, S. Ponomarev, L. Shekhtman, K. Ten, B. Tolochko, I. Zhogin, and V. Zhulanov, Nucl. Instrum. Methods Phys. Res., Sect. A **513**, 388 (2003). https://www.doi.org/10.1016/j.nima.2003.08.067
6. A. Aulchenko, V. Zhulanov, L. Shekhtman, B. Tolochko, I. Zhogin, O. Evdokov, K. Ten, Nucl. Instrum. Methods Phys. Res., Sect. A **543**, 350 (2005). https://www.doi.org/10.1016/j.nima.2005.01.254
7. V. M. Aulchenko, O. V. Evdokov, L. I. Shekhtman, K. A. Ten, B. P. Tolochko, I. L. Zhogin, and V. V. Zhulanov, J. Instrum. **3**, P05005 (2008). https://www.doi.org/10.1088/1748-0221/3/05/P05005
8. V. M. Aulchenko, O. V. Evdokov, L. I. Shekhtman, K. A. Ten, B. P. Tolochko, I. L. Zhogin, V. V. Zhulanov, Nucl. Instrum. Methods Phys. Res., Sect. A **603**, 73 (2009). https://www.doi.org/10.1016/j.nima.2008.12.163
9. V. M. Aulchenko, S. E. Baru, O. V. Evdokov, V. V. Leonov, P. A. Papushev, V. V. Porosev, G. A. Savinov, M. R. Sharafutdinov, L. I. Shekhtman, K. A. Ten, V. M. Titov, B. P. Tolochko, A. V. Vasiljev, and I. L. Zhogin, Nucl. Instrum. Methods Phys. Res., Sect. A **623**, 600 (2010). https://www.doi.org/10.1016/j.nima.2010.03.083
10. K. A. Ten, E. R. Pruuel, L. A. Merzhievsky, L. A. Lukjanchikov, B. P. Tolochko, I. L. Zhogin, and L. I. Shekhtman, Nucl. Instrum. Methods Phys. Res., Sect. A **603**, 160 (2009). https://www.doi.org/10.1016/j.nima.2008.12.192
11. V. M. Titov, E. R. Pruuel, K. A. Ten, L. A. Luk'yanchikov, L. A. Merzhievskii, B. P. Tolochko, V. V. Zhulanov, and L. I. Shekhtman, Combust., Explos. Shock Waves **47**, 615 (2011). https://www.doi.org/10.1134/S0010508211060013
12. E. R. Pruuel, K. A. Ten, B. P. Tolochko, L. A. Merzhievskii, L. A. Luk'yanchikov, V. M. Aul'chenko, V. V. Zhulanov, L. I. Shekhtman, and V. M. Titov, Dokl. Phys. **58**, 24 (2013). https://www.doi.org/10.1134/S1028335813010035
13. K. A. Ten, E. R. Pruuel, A. O. Kashkarov, I. A. Rubtsov, M. V. Antipov, A. B. Georgievskaya, A. L. Mikhailov, I. A. Spirin, V. M. Aulchenko, L. I. Shekhtman, V. V. Zhulanov, and B. P. Tolochko, Combust., Explos. Shock Waves **54**, 606 (2018). https://www.doi.org/10.1134/S0010508218050143
14. L. I. Shekhtmana, V. M. Aulchenko, V. N. Kudryavtsev, V. D. Kutovenko, V. M. Titov, V. V. Zhulanova, E. L. Pruuel, K. A. Ten, and B. P. Tolochko, Phys. Procedia **84**, 189 (2016). https://www.doi.org/10.1016/j.phpro.2016.11.033

15. V. Aulchenko, E. Pruuel, L. Shekhtman, K. Ten, B. Tolochko, and V. Zhulanov, Nucl. Instrum. Methods Phys. Res., Sect. A **845**, 169 (2017). https://www.doi.org/10.1016/j.nima.2016.05.096

16. L. I. Shekhtman, V. M. Aulchenko, V. V. Zhulanov, and D. V. Kudashkin, Bull. Russ. Acad. Sci.: Phys. **83**, 220 (2019). https://www.doi.org/10.3103/S1062873819020254

17. L. Shekhtman, V. Aulchenko, V. Kudryavtsev, V. Kutovenko, V. Titov, and V. Zhulanov, AIP Conf. Proc. **2299**, 050004 (2020). https://www.doi.org/10.1063/5.0030393

18. L. Shekhtman, V. Aulchenko, D. Kudashkin, V. Kudryavtsev, E. Pruuel, K. Ten, B. Tolochko, and V. Zhulanov, Nucl. Instrum. Methods Phys. Res., Sect. A **958**, 162655 (2020). https://www.doi.org/10.1016/j.nima.2019.162655

19. V. M. Aulchenko, L. I. Shekhtman, and V. V. Zhulanov, Optoelectron., Instrum. Data Process. **56**, 81 (2020). https://www.doi.org/10.3103/S8756699020010112

Translated by A. Ivanov